 doi:10.20944/preprints202205.0140.v1

Article

Modeling of Multiple Fatigue Cracks for Aircraft Wing Corner Box Based on Non-ordinary Sate Peridynamics

Junzhao Han [1], Guozhong Wang [2*], Xiaoyu Zhao [3*],Rong Chen [1] and Wenhua Chen [1,*]

[1] School of Mechanical Engineering and Automation, Zhejiang Sci-Tech University, Hangzhou 310018, P. R. China; hanjz@zju.edu.cn
[2] Henghong Intelligent Equipment Co.,Ltd, Hangzhou 310018, P. R. China; gzwang@hzjx.com.cn
[3] China Ship Scientific Research Center, Wuxi, Jiangsu, 214028, P. R. China; zhxiyu123@126.com
* Correspondence: chenwh8@zju.edu.cn;

Abstract: In this work, we have developed a non-ordinary state-based peridynamic model for multiple crack initiation and propagation due to compression-compression fatigue load. In each loading cycle, the fatigue loading is redistributed among the peridynamic solid body, leading to the progressive fatigue damage initiation and propagation in an autonomous fashion. The proposed fatigue model parameters are firstly validated by 3D numerical benchmark tests, and then it is applied to simulate widespread fatigue damage evolution of the aircraft wing corner box. The modified constitutive damage model has been implemented into the peridynamics framework at finite strain. Furthermore, the criterion algorithm from multiple initiation to propagation is discussed. It is shown that the numerical results obtained from peridynamics simulations are in general agreement with those from the experiment data. The comparison of experimental and numerical results indicates that the proposed non-ordinary state-based peridynamics fatigue model has the ability to capture the multiple crack initiation and propagation and other features of the aluminium alloy material.

Keywords: Non-ordinary state-based Peridynamics; Compression-compression fatigue load; Multiple Cracks; Aircraft wing corner box

1. Introduction

Extensive fatigue damage of aging aircraft structures has aroused wide attention in the aerospace area. The fatigue initiation and propagation prediction of the structure are a complicated, tough work because of the uncertain loads and uncertainties in material properties. The fatigue damage law should be deduced to ensure the flight safety and improve the economic cost. In materials science, fatigue is the initiation and propagation of cracks in a material due to cyclic loading. Once a fatigue crack has initiated, it grows a small amount with each loading cycle, typically producing striations on some parts of the fracture surface. The crack will continue to grow until it reaches a critical size, which occurs when the stress intensity factor of the crack exceeds the fracture toughness of the material, producing rapid propagation and typically complete fracture of the structure. Fatigue of metallic structures is a cumulative irreversible process that occurs due to the internal friction, initiation and growth of micro-fractures[1-3]. Vacancies generated when an atom or an ion missing from its regular crystallographic site and new equilibriums is built. Under repeated loading, the new dynamic equilibriums lost to generate the next balances, and then the fatigue damage initiates and accumulates in a natural way[4-6]. Therefore, metal fatigue process includes complex submicroscopic and microscopic damage propagation[7-9]. The fatigue life of metal structures under cyclic loading can be accurately predicted from crack initiation to propagation, which is influenced by the material properties, geometric parameter, boundary loads, external environment, etc. The whole process of fatigue is essentially a complex multi-scale phenomenon which has important features at multiple scales of time and/or space[10-14]. Therefore, the prediction

 doi:10.20944/preprints202205.0140.v1

of fatigue damage in metallic materials encounter many problems[15-17]. The classical continuum mechanics theory, using spatial partial differential equations (SPDE), especially the finite element method (FEM), has been used to predict fatigue crack growth in materials under cyclic loading[18,19]. Based on the framework of traditional continuum theory, the FEM model or various modified versions aim to find the kinetic relations among parameters near the fatigue crack tip that characterize the fatigue crack evolution[20-22]. The main barrier is that these models can't directly perform on the fatigue crack tips or crack surfaces. Instead, by redefining the body, the crack is treated as a boundary so that extra criteria, such as fatigue crack growth speed and direction which guide the crack path, are necessary[23-25]. In order to deal with those problems, Linear Elastic Fracture Mechanics (LEFM) use Cohesive Zone Elements (CZE) to deal with Mode-I crack model and mixed-model fracture. The number of cohesive elements increases with decreasing mesh size, yet the size of the continuum region remains the same. Fatigue crack growth shows the mesh dependence property, and a special remeshing technique is required. Frequent redefining the body is difficult and costly, especially with multiple interacting cracks. The extended finite element method (XFEM), using the local enrich functions, permits the cracks to propagate on any element surface without remeshing in every incremental crack growth. Neither FEM model or various modified versions nor the XFEM method suffers from the need to supply extra criteria such as the time of forming fatigue cracks, fatigue propagation speed, direction, branch, arrest, etc. In other words, fatigue crack initiation and fatigue crack propagation are treated separately by coupling dissimilar mathematical systems under the framework of traditional continuum theory. The final fatigue fracture mechanisms are associated with grain boundaries, dislocations, microcracks, anisotropy, etc[26-30]. Each of which plays an important role at a specific length scale. It is difficult to obtain the location of fatigue initiation in advance, let alone the extra criteria from the experimental data[31-36].

Despite the development of many important concepts to predict crack initiation and its growth in materials and structures, it is still a major challenge within the framework of classical continuum mechanics. The main difficulty lies in the mathematical formulation, which assumes that a body remains continuous as it deforms. Therefore, the basic mathematical structure of the formulation breaks down whenever a discontinuity appears in a body. Mathematically, the classical theory is formulated using spatial partial differential equations, and these spatial derivatives are undefined at discontinuities. This introduces an inherent limitation to the classical theory, as the spatial derivatives in the governing equations, by definition, lose their meaning in the presence of a discontinuity, such as a crack[37]. Because traditional numerical methods such as the finite element and boundary methods rarely obtain solutions to these problems, a mesh-free method seems more appropriate. To develop an accurate numerical model and obtain reliable results in numerical simulation, the material–failure model should satisfy two main criteria[38]. First, the model must be able to predict the correct stresses and strains in failure. Second, the predicted failure mechanism and fracture pattern must be in accordance with those found in experiments. A discrete method has advantages for modeling the discontinuous phase of the fracture process, but accuracy problems during the continuous phase make it unreliable for modeling the whole process, from continuous to discontinuous. A new mesh-free method called peridynamics was coined by Silling in 1998. This theory is a reformulation of the classical continuum mechanics that employs a nonlocal model to describe material properties. It assumes that particles in a continuum interact across a finite distance, and it formulates problems in terms of integral equations rather than partial differential equations. Peridynamics manifests its unique superiority in addressing discontinuous problems, which can be introduced to the calculation and simulation of fatigue loads. In contrast, a peridynamic theory (PD) uses the spatial integral equations as opposed to derivatives of the displacement field to compute internal force acting on a material particle[39-41]. Material damage is part of the constitutive model. Without the need for special crack growth criteria, peridynamics allows the cracks to propagate at multiple sites with natural paths not only along the element boundary in a consistent framework. Furthermore, the

Preprints (www.preprints.org) | NOT PEER-REVIEWED | Posted: 10 May 2022 doi:10.20944/preprints202205.0140.v1

PD theory can link the micro to macro length scales[42-44]. This formulation allows us to model crack initiation, propagation, branching and coalescence without special assumptions.

The fatigue crack model with peridyanmic was originally proposed by Oterkus, Guven, and Madenci[45] and substantially improved by Askari[46]. Two phases of fatigue failure: crack initiation, fatigue propagation, is included in a consistent fatigue model and the parameters of the model are calibrated separately with experimental data. In ref[46], the dynamic relaxation method is used to obtain the static solution. Nucleation and growth of a helical fatigue crack are demonstrated by using an aluminum alloy rod. Zhang[47] presented the conjugate gradient energy minimization method to obtain the static solution and applied this fatigue model to two-phase composite materials. The results show that the peridynamic fatigue crack model can deal with multiple crack without extra criteria to guide the crack path[48-51].

In the present investigation, a non-ordinary state-based peridynamics fatigue model is applied for the first time in the calculation of compression-compression loads and the simulation of the multiple crack initiation and propagation. The basic non-ordinary state-based peridynamics theory is introduced, including the peridynamics model of a continuum; and constitutive modeling that obtains the microscopic parameters and the description of fatigue failure. Based on the thermal disturbance of atomic motion, the theoretical foundation for the peridynamic fatigue model is built under cyclic loading. To bridge the micro fatigue crack initiation to the macro fatigue crack growth, an alternative non-ordinary state-based peridynamic model for multiple fatigue cracking is presented. Fatigue model parameters are verified from experimental data of aluminium alloy material. Each bond in the deformed material configuration is treated as a fatigue test subjected to fatigue loads. Bond damage accumulated over time, according to the cyclic strain in the bond that its progressive failure is characterized by a history variable called “wear-out life”. A bond is broken when the variable reaches the entire life. Fatigue crack initiation and crack growth formulated naturally over many loading cycles which is controlled by the parameter “node damage” within a region of finite radius. Critical damage factors are also imposed to improve efficiency and stability for the fatigue model. Based on the improved adaptive dynamic relaxation method, the static solution is obtained in every loading cycle. Convergence analysis is presented in the aircraft wing corner box at different loading levels. Experimental results show that the peridynamic results capture the multicrack sensitive location well without extra criteria. Fatigue lifetimes obtained from the simulation have a good correlation with the experimental results.

2. Progressive Fatigue Damage Evolution

2.1. Microscopic Fatigue Crack Initiation and Propagation

Understanding of cumulative damage mechanisms is essential since it provides the necessary physical bases for modeling the cumulative damage process. Atoms vibrate in frequency (about 1012~1013Hz) and small amplitude surrounding equilibrium position based on crystallographic theory. Each atom in the material has certain energy which keeps it in dynamic balance state. When the dynamic balance state of an atom is broken, the atom will jump out of its original equilibrium position and a vacancy will be generated. The probability of an atom’s active energy reaching to the critical value Q_c because of thermal disturbance motion can be expressed as

$$P_c = \exp\left(-Q_c / kT\right) \tag{1}$$

where k is a physical Boltzmann constant with respect to temperature and energy, T is the representation of average kinetic energy of atom, and Q_c is the critical active energy that is smallest value of an atom escaping from the equilibrium position.

As shown in Fig. 1(a), although the critical activity Q_c is larger than other loading conditions, there is still has a certain probability of leaving the original equilibrium position and entering the new equilibrium position, for the escape probability of the atom in all directions is the same. Therefore, in a dynamic equilibrium state of crystal vacancies,

Preprints (www.preprints.org) | NOT PEER-REVIEWED | Posted: 10 May 2022 doi:10.20944/preprints202205.0140.v1

no fixed crystal defects will be formed and there will be no damage evolution formed without external loading.

As shown in Fig. 1(b), under static load, the critical active energy Q_c is inversely proportional to the stress level. The higher the stress, the smaller the critical active energy is. Therefore, the atom has a higher probability of having energy above this critical active energy. Based on this theory, the critical active energy Q_c is described as follows

$$Q_c = \begin{cases} \dfrac{\tau_b^2 + \alpha\tau_b\tau + \beta\tau^2}{2G} & static\ \ loading \\ \dfrac{\tau_b^2}{2G} & no\ external\ loading \end{cases} \tag{2}$$

where τ_b is ideal shear strength for material, τ is the external shear stress, G is the shear modulus, α is physical constant correlated with stress concentration factor, β is physical constant correlated with load amplitude, and $\alpha\tau_b\tau + \beta\tau^2 \le 0$.

Combining Eq. (1) and Eq. (2), the probability of an atom's active energy reaching to the critical value Q_c under static load can be expressed as

$$P_c = \exp\left(-\frac{\tau_b^2 + \alpha\tau_b\tau + \beta\tau^2}{2GkT}\right) \tag{3}$$

where it is obviously that the probability of an atom with static loading escaping from the equilibrium position is larger than the condition without external load. Since the displacement u_0 of an atom away from the equilibrium position is fixed at this time, escaping probability of the atom in all directions is the same with respect to the new equilibrium position. Therefore, the vacancies generated by atomic escape by the thermal disturbance can be annihilated. Vacancies generated by atomic escape show mutual annihilation without accumulating to form defects or make defects grow. Therefore, there will be no damage evolution formed under static load.

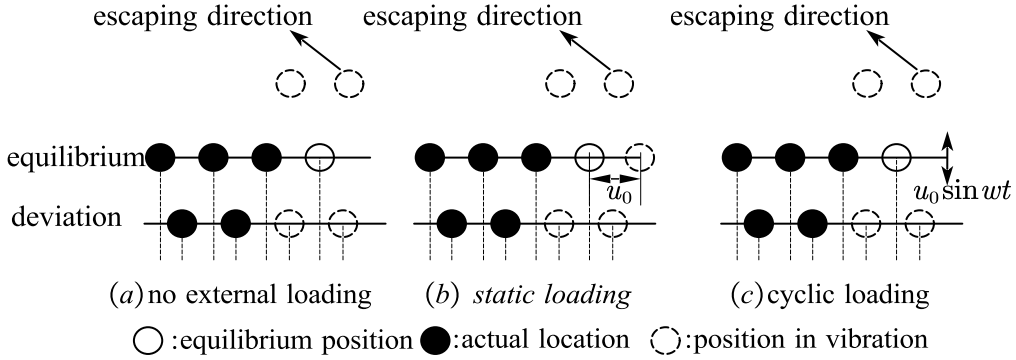

Figure 1. The thermal disturbance of atomic motion under different loading condition

As shown in Fig. 1(c), under cyclic loading, the equilibrium position is constantly changing during the deformation process. The atomic escaping direction is isotropic with respect to the instantaneous equilibrium position. However, the motion of the equilibrium position itself will destroy this isotropic property. The displacement of an atom away from the original equilibrium position is alternating. The voids generated by the thermal disturbance cannot be annihilated so that the damage will be initiated and accumulated.

According to the above analysis, we can see that atomic vacancies generated by the thermal disturbance cannot completely annihilate with each other due to the change of the equilibrium position itself. And the thermal disturbance forms a defect or causes its development.

As shown in Fig. 2, under cyclic loading, fatigue damage evolution preferentially forms at grain boundaries. Fatigue occurs at stress amplitude below the yield stress. Fatigue crack initiation and propagation are a consequence of cyclic slip. It implies cyclic plastic deformation, or in other words dislocation activities. Progressive damage models are often based on damage mechanics concepts. Therefore, this view provides the way to

Preprints (www.preprints.org) | NOT PEER-REVIEWED | Posted: 10 May 2022 doi:10.20944/preprints202205.0140.v1

set up the damage evolution law with theoretical foundation. The evolution law based on this mechanism can well indicate the already known damage-life relationships of metals.

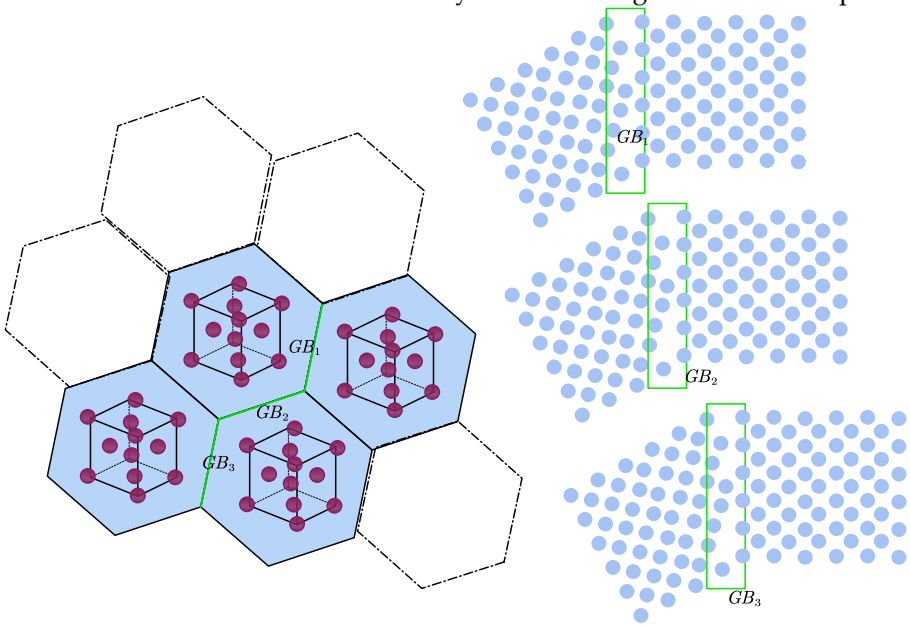

Figure 2. Grain boundary damage indued by cyclic loading

2.2. Widespread Fatigue Damage

Widespread fatigue damage (WFD) has become the focus of research in aviation. The extensive fatigue damage can be divided into two forms: multi-component damage and multi-site damage. The traditional damage tolerance analysis is not applicable to the extensive fatigue damage structure, and the interaction between multiple cracks in WFD structure makes the damage tolerance assessment of the structure complicated. The key point to deal with those problem is to know that fatigue damage accumulation equals to the energy non-uniform dissipation process. A certain amount of energy must be provided to overcome the binding energy within or between grain boundaries for material fatigue damage.

As shown in Fig. 3, the hysteresis-loop area is equal to deformation work produced during one loading cycle. This deformation work is mainly transformed into heat energy, and a very small part of it into stored energy. The total hysteresis energy is then equal to the sum of areas of all hysteresis loops. If we neglect the hardening/softening, the total energy can be expressed as the product of the area of the saturation hysteresis loop and the number of cycles to fracture. This has been utilized in some energy-based theories of the fatigue process, and thence the area of the stable hysteresis loop becomes an important quantity. The hysteresis-loop area can be generally expressed as

$$\Delta W = \iint d\sigma d\varepsilon_p = \oint \sigma(\varepsilon_p) d\varepsilon_p \tag{4}$$

where ΔW is loop area, σ is the stress and ε_p is the strain.

Under cyclic loading, the widespread fatigue damage can be described as

$$\sum_{i=1}^{n} \Delta S_i = c_1 \sum_{i=1}^{n} \Delta W_i + c_2 \sum_{i=1}^{n} \Delta U_i + \ldots \tag{5}$$

Preprints (www.preprints.org) | NOT PEER-REVIEWED | Posted: 10 May 2022 doi:10.20944/preprints202205.0140.v1

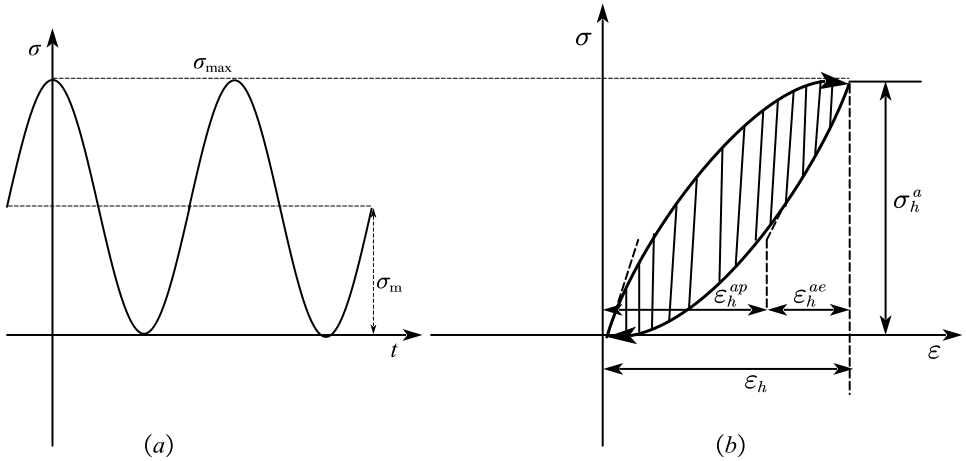

Figure 3. Schematic representation of (a) sinusoidal fatigue loading with a mean stress as stress σ_m vs. time plot and (b) corresponding stress-strain hysteresis loop with definition of the main parameters

2.3. Fatigue Damage Accumulation for Multiple Crack

Cumulative damage process of materials is a nonlinear process of interaction between loading stress and damage accumulation. Three-dimensional damage accumulation model can be expressed as

$$\hbar_D^* = \frac{\varsigma_1}{\varsigma_2 + 1}\left(-\frac{\psi}{\varsigma_1}\right)^{\varsigma_1+1}(\dot{\varpi} + \dot{c}) / (1-D)^T \tag{6}$$

where $\hbar_D^*$ is the thermodynamics dissipative potential under cyclic loading conditions, ς_1, ς_2, and T are material parameters depend on thermodynamic temperature, $\dot{\varpi}$ is accumulative plastic strain rate, $\dot{c}$ is microplasticity strain rate, ψ is damage strain energy release rate. Based on the compression-compression loading theory, the damage strain energy release rate is described as follows

$$\psi = -\frac{e_{eq}\varsigma_i}{2E(1-D)^2} \tag{7}$$

where e_{eq} is Von Mises equivalent stress, ς_i is stress triaxial factor, D is damage variable, E is elastic modulus. The stress triaxial factor can be expressed as

$$\varsigma_i = \frac{2}{3}(1+\nu) + 3(1-2\nu)\left(\frac{e_H}{e_{eq}}\right)^2 \tag{8}$$

where e_H is hydrostatic pressure, ν is Poisson's ratio.

Based on orthogonality principles, the damage variable rate can be described as follows

$$\dot{D} = -\frac{\partial \hbar_D^*}{\partial \psi} = \left(-\frac{\psi}{\varsigma_1}\right)^{\varsigma_1}(\dot{\varpi} + \dot{c}) / (1-D)^T \tag{9}$$

3. State-based Peridynamics for Multiple Cracking

3.1. The Motion and Deformation of a Material Point

Cumulative damage process of materials is a nonlinear process of interaction between loading stress and damage accumulation. Three-dimensional damage accumulation model can be expressed as

$$\rho(\boldsymbol{x})\ddot{\boldsymbol{u}}(\boldsymbol{x},t) = \int_{H_x} (\boldsymbol{t}(\boldsymbol{u}'-\boldsymbol{u}, \boldsymbol{x}'-\boldsymbol{x}, t) - \boldsymbol{t}'(\boldsymbol{u}-\boldsymbol{u}', \boldsymbol{x}-\boldsymbol{x}', t))dH_x + \boldsymbol{b}(\boldsymbol{x},t) \tag{10}$$

where $\rho(\boldsymbol{x})$ represents the mass density in the reference configuration, $\boldsymbol{x}$ represents the vector of coordinates, $\boldsymbol{u}$ and $\boldsymbol{u}'$ represent acceleration and displacement vectors, respectively. In PD, the external loads are applied to the model by using the vector of body forces, $\boldsymbol{b}(\boldsymbol{x},t)$. The motion of the material point conforms to the Lagrangian description.

Preprints (www.preprints.org) | NOT PEER-REVIEWED | Posted: 10 May 2022 doi:10.20944/preprints202205.0140.v1

As shown in Fig. 4, the motion of a material point in PD is influenced by collective deformations of surrounding material points within a domain which is called horizon, H_x. In the 3D model, the horizon of material point is defined as the sphere with a radius surrounding that material point. Here, δ is called the horizon size. Material points within the horizon of a material point are called family members of that material point.

$$\begin{cases} \underline{\mathbf{Y}}\left(\boldsymbol{x}_{(k)},t\right)=\begin{Bmatrix} \boldsymbol{y}_{(1)}-\boldsymbol{y}_{(k)} \\ \vdots \\ \boldsymbol{y}_{(\infty)}-\boldsymbol{y}_{(k)} \end{Bmatrix} \\ \left(\boldsymbol{y}_{(j)}-\boldsymbol{y}_{(k)}\right)=\underline{\mathbf{Y}}\left(\boldsymbol{x}_{(k)},t\right)\langle \boldsymbol{x}_{(1)}-\boldsymbol{x}_{(k)}\rangle=\boldsymbol{F}\left(\boldsymbol{x}_{(j)}-\boldsymbol{x}_{(k)}\right) \end{cases} \tag{11}$$

where all the $\left(\boldsymbol{y}_{(j)}-\boldsymbol{y}_{(k)}\right)$ vectors can be stored in an infinite-dimensional array, or a vector state, $\underline{\mathbf{Y}}\left(\boldsymbol{x}_{(k)},t\right)$. There is a direct relationship between the vector state $\underline{\mathbf{Y}}$ and the second-order tensor $\boldsymbol{F}$. This relationship can be expressed as the "expansion" of the second-order tensor.

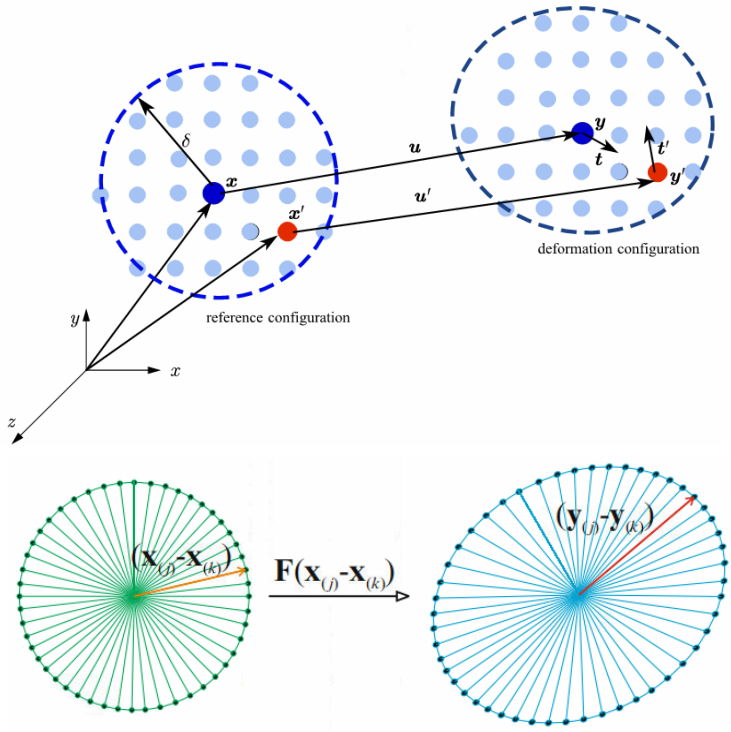

Figure 4. Deformation of vector state and kinematic of PD material point

As shown in Fig. 5, peridynamics(PD) theory is analogous to molecular dynamics(MD), where the interaction between material points and is called a bond, which one can view as a spring in the case of elastic interaction. The property of a bond that shows interaction over a finite distance is a fundamental difference between peridynamics theory and classical theory. PD theory describes the interaction process of material points in space by nonlocal method. Fatigue cracks are naturally included in the space integral motion control equation (SIE). Elastic-plastic fracture mechanics (EPFM) theory characterizes the stress-strain response process of material points by local method. Fatigue cracks are treated as boundary conditions of structural components or space partial differential motion control equation (SPDE).

Preprints (www.preprints.org) | NOT PEER-REVIEWED | Posted: 10 May 2022 doi:10.20944/preprints202205.0140.v1

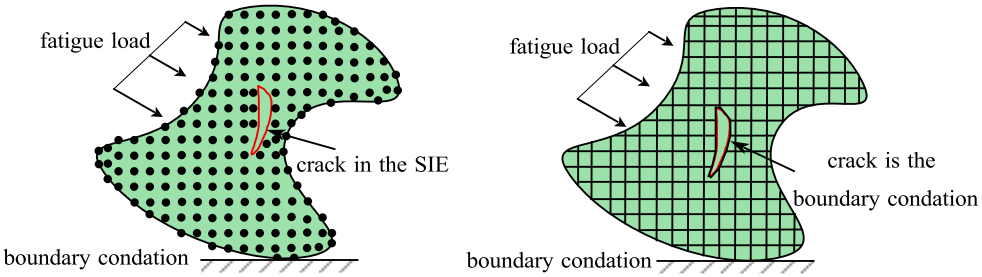

(a) cracks in the SIE (b) cracks are the boundary

Figure 5. PD and EPFM

3.2. Energy-based Fatigue Model

The method of crack nucleation and propagation within the peridynamic model is through the permanent breaking of bonds. The word bond is used loosely in this context only to describe the relationship between two material points and can be thought of abstractly as an interaction potential; There is not necessarily a notion of direct connectivity such as a spring-like force. As shown in Fig. 6, the force vector states $\underline{\mathrm{T}}[x_{(k)},t]$ and $\mathrm{T}[x_{(j)},t]$ are not parallel to their deformed relative position and their values are not equal. Therefore, a failure model derived from thermodynamic notions of energy is developed. The amount of energy density stored in a bond ξ can be performed as follows

$$\psi_{\xi}=\int_{\eta(t_1)}^{\eta(t_2)}\{\underline{\mathrm{T}}[\boldsymbol{x}_{(k)},t]\langle x_{(j)}-x_{(k)}\rangle-\underline{\mathrm{T}}[\boldsymbol{x}_{(j)},t]\langle x_{(k)}-x_{(j)}\rangle\}\cdot d\boldsymbol{\eta} \tag{12}$$

where ψ_{ξ} represents units of energy per unit volume squared. The amount of work density done on the bond ξ due to displacing the material points $\boldsymbol{x}_{(k)}$ and $\boldsymbol{x}_{(j)}$ relative to one another from $\eta(t_1)$ to some final scalar value of displacement, $\eta(t_2)$, which is a function of time. This projection neglects any work done on the points due to rigid body translation. The motivation for this idea comes from the well-known physics equation where the work done to a body is the force acting on it, $\boldsymbol{F}$, integrated over the path length, $\boldsymbol{s}$, as shown in Eq..

$$W_s=\int \boldsymbol{F}\cdot d\boldsymbol{s} \tag{13}$$

Compared with Eq. (12) and Eq. (13), it is clear that the work W_s is an energy density, the force $\boldsymbol{F}$ is the dual force density, and the path $\boldsymbol{s}$ is the relative displacement.

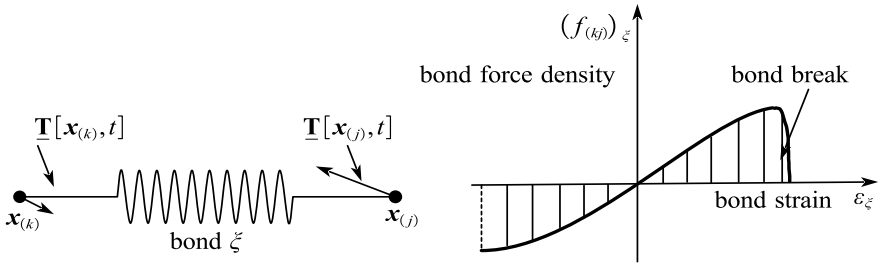

(a) (b)

Figure 6. Bond damage and energy density

As shown in Fig. 6, the force density $f_{(kj)}=(\underline{t}[x_{(k)},t]-\underline{t}[x_{(j)},t])$ exhibits non-linearity under cycle loading, therefore the total energy density stored in the bond ξ can be expressed as follows.

$$\omega_{\xi}=\int_0^{\varepsilon_{\xi}(\Delta t)}\left(f_{(kj)}\right)_{\xi}\,d\varepsilon \tag{14}$$

Preprints (www.preprints.org) | NOT PEER-REVIEWED | Posted: 10 May 2022 doi:10.20944/preprints202205.0140.v1

3.3. Fatigue Crack Tip Deformation Analysis

As shown in Fig. 7(a), there are three kinds of bonds near the model-I crack tip: broken bonds, core bonds, and partially damaged bonds. For the core bonds, the bond strain s_{core}^{*} is the largest compared with the partially damaged bonds. Since the material is linear elastic-perfectly plasticity, the core bond strain can be described as

$$s_{core}^{*}(\delta)=\hat{s}_{core}\frac{\hat{\lambda}}{E\sqrt{\delta}} \tag{15}$$

where $\hat{\lambda}$ is the stress intensity factor, E is elastic modulus, $\hat{s}_{core}$ is a dimensionless parameter.

As shown Fig. 7(b), there is a plastic zone near the crack tip, the length of the plastic zone is r_p^{*}. For the linear elastic fracture mechanics, the strain in the plastic zone can be described as

$$s(z)=\frac{\hat{\lambda}}{E\sqrt{2\pi z}}\ (0\leqslant z\leqslant r_p^{*}) \tag{16}$$

Combining Eq. (15) and Eq. (16), a function $\hat{f}$ can be described as

$$\hat{f}\left(\frac{z}{\delta}\right)=\frac{1}{\hat{s}_{core}\sqrt{2\pi z/\delta}} \tag{17}$$

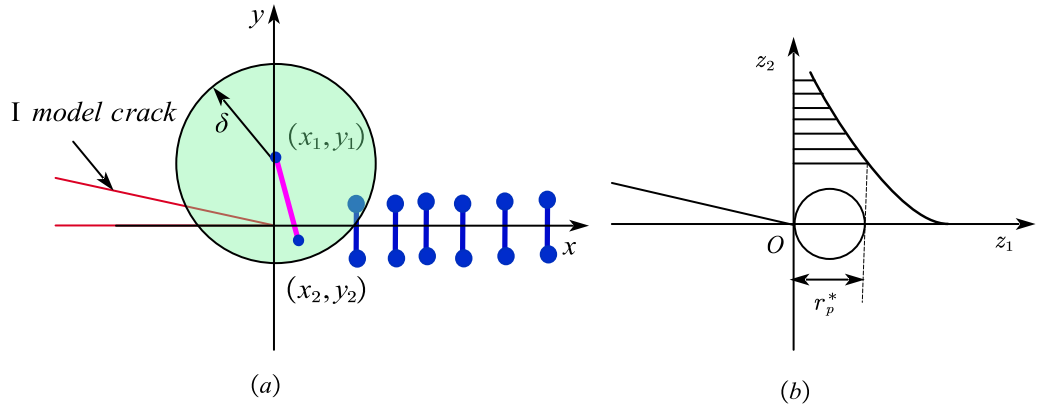

Figure 7. Crack tip analysis with I model crack

4. Fatigue Model Based on Non-ordinary State-based Peridynamics

In ref.[46], Silling and Askari proposed a bond damage model within peridynamics to treat the nucleation and growth of cracks due to cyclic loading. The bond-based fatigue constitutive model contains two phases in the fatigue crack process, crack initiation and crack propagation by using different choices of the parameters. For the crack initiation process, the crack initiate from the first bond which the evolution law is characterized by a damage variable "remaining life", that evolves over time. For the crack propagation, the crack follows Paris' law during the fatigue crack growth phase. Inspired by this work, in Ref.[53], a trans-scale ordinary state-based peridynamic fatigue model is built based on the mechanism of fatigue. Macroscale is directly dicted by the tans-scale peridyanmic model. Each bond in the body is defined as the ideal fatigue test specimen under variable loads.

4.1. Progressive Failure in the Non-ordinary State-Based Peridynamic Body

Material particles in non-ordinary state-based peridynamic solid are connected via physical interactions. As elimination of physical interactions among the material points, material damage is introduced. Meanwhile, the spring like bond between two particles, *k* and *j*, break in an irreversible manner. Obviously, the bond strain exceeds its critical value and the micro-potential between the two material points will be removed away. Therefore, the fatigue loading is redistributed among the peridynamic solid body in every cycle, leading to the progressive fatigue damage initiation and propagation in an autonomous

Preprints (www.preprints.org) | NOT PEER-REVIEWED | Posted: 10 May 2022 doi:10.20944/preprints202205.0140.v1

fashion. As shown in Fig. 8(a), the spring like bond ξ_{kj} is subjected to force density in its two ends during compression-compression loading cycle exert on the peridynamic solid body. The progressive fatigue bond damage can be performed as follows

$$D_{kj}(\xi_{kj},t)=\begin{cases}1, & if\ \xi_{kj}\ is\ broken\\ \mathcal{G}(\xi_{kj},s_{kj},t), & otherwise\end{cases} \tag{18}$$

where $\mathcal{G}(\xi_{kj},s_{kj},t)$ is a normalized bond damage function, depending on the current bond deformation s_{kj} and the history time t.

As shown in Fig. 8(b), for a given material particle $x_{(k)}$, the bond 1^k, 2^k, 3^k within its horizon family $H_{x(k)}$ break in sequence and the physical interactions of the two particles vanished. As for the material particle $x_{(j)}$, the bond 4^k within its horizon family $H_{x(j)}$ break after other three bonds breaking. The four broken bonds show the crack surface $\mathcal{P}_{crack}$ and its direction is the way in which arrow point. Therefore, the fatigue damage of a particle within its horizon family under compression-compression fatigue loading can be described as

$$D_k\left(x_{(k)}\right)=\frac{\int_{H_{x(k)}}\mathcal{G}(\xi_{kj},s_{kj},t)dV^k}{\int_{H_{x(k)}}dV^k} \tag{19}$$

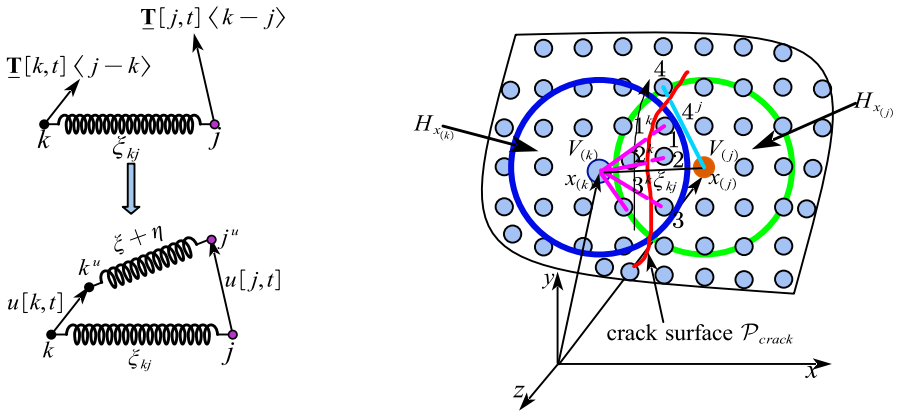

(a) Particles motion and bond ξ_{kj} defomation (b) Progressive failure leading to crack suface $\mathcal{P}_{crack}$

Figure 8. Bond deformation and crack surface in PD configuration

4.2. Multiscale Fatigue Model for multi-crack process

Metal fatigue failure is a cross-scale damage evolution process involving many physical levels. The introduction of multiscale method promotes the establishment of fatigue model based on physical mechanism. However, there are still some problems in the research of multi-scale fatigue, such as the imperfect theory of cross-scale correlation mechanics and the lack of effective method of cross-scale experiment characterization. The whole process of fatigue, crack initiation and followed by slow crack propagation, shows a trans-scale characteristic, which is mainly manifested in time and space. Over the time scale, from millisecond to year, progressive fatigue damage brings crack initiation and propagation. Over the space scale, fatigue crack length characterizes from micrometer to meter.

As shown in Fig. 9(b), 3D geometric specimen undergoes compression-compression fatigue loading acting on the boundary layer region. The boundary layer region is discretized into material particles and uniform load were performed on each discrete material points in the boundary layer region(as shown in Fig. 9(c)). For a given bond ξ in the peridynamic solid, as shown in Fig. 10(a) and (b), the force density acting on the spring-like bond ξ varies in a noncyclic way. The spectrum loading of the bond strain in the peridynamic solid body varies irregularly during each loading cycle, shown in Fig. 10(c).

Preprints (www.preprints.org) | NOT PEER-REVIEWED | Posted: 10 May 2022 doi:10.20944/preprints202205.0140.v1

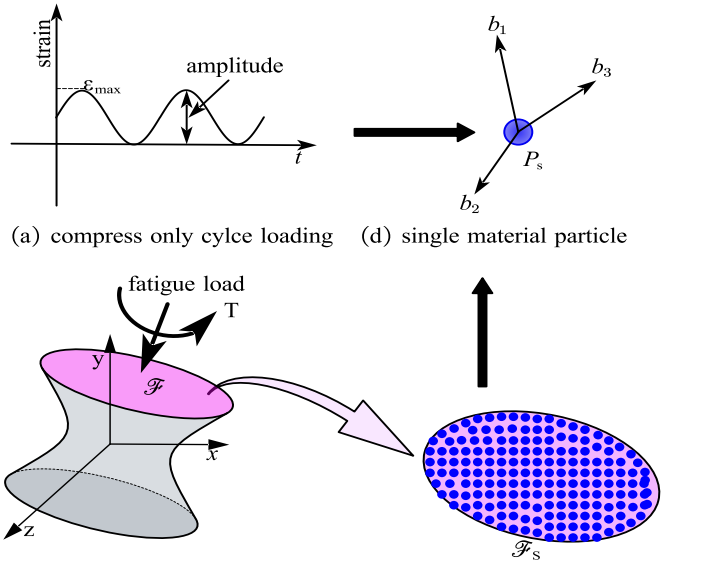

Figure 9. Fatigue loading on the boundary layer region

Therefore, in a classic local model a material point only exchanges mass, momentum, and energy with its closest neighbors. As a result, in classical mechanics the stress state at a point depends on the deformation at that point only. The validity of this assumption becomes questionable across different length scales. The field of fracture mechanics is primarily concerned with the evolution of pre-existing cracks within a body, rather than the nucleation of new cracks. In general, at the macroscale this assumption is acceptable. However, the existence of long-range forces is evident from the atomic theory and as such the supposition of local interactions breaks down as the geometric length scale becomes smaller and approaches the atomic scale. Even at the macroscale there are situations when the validity of locality is questionable, for instance when small features and microstructures influence the entire macrostructure.

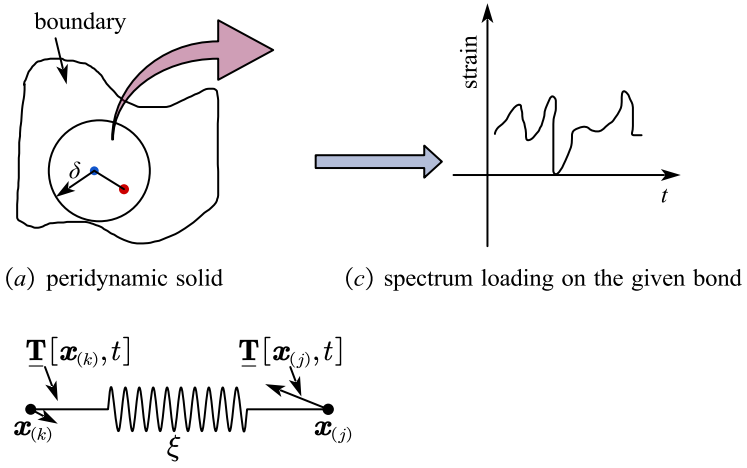

Figure 10. Spectrum loading on the material point during loading cycle

In order to express the damage accumulation rate of the bond ξ explicitly, the concise representation of the critical active energy $Q(\sigma_a,\sigma_m,D)$ is obtained by using inverse analysis through the wide spread fatigue damage and microscopic fatigue crack initiation and propagation law.

The normalized fatigue damage quantity of bond ξ can be expressed by fictious time t_f, as follows

Preprints (www.preprints.org) | NOT PEER-REVIEWED | Posted: 10 May 2022 doi:10.20944/preprints202205.0140.v1

$$\begin{cases} \lambda(\boldsymbol{x},\xi,t_f) = N[1-(1-D)^{B+1}]^{A(\tilde{\sigma})}(\dfrac{\sigma_a}{M(\bar{\sigma})(1-D)})^B \\ t_f = \dfrac{N}{N_f} \end{cases} \tag{20}$$

where N_f is the cycle number to failure, N is the current cycle number, $M(\bar{\sigma})$ is function of average stress, $A(\tilde{\sigma})$ is function of alternating stress, B is material characteristic coefficient related to temperature. The normalized fatigue damage quantity $\lambda(\boldsymbol{x},\xi,t_f)$ is defined as the consumption life of the bond. It involves the loading cycle N increases. The bond breaks at the loading cycle N that

$$\lambda(N) \geq 1 \tag{21}$$

The first bond in the entire domain breaks with is the cyclic strain range.

$$N_1[1-(1-D_c)^{B+1}]^{A(\tilde{\sigma})}(\frac{\sigma_a}{M(\bar{\sigma})(1-D_c)})^B = 1 \tag{22}$$

where N_1 is the smallest cycle at which this bond breaks and $\lambda(N_1)=1$. The first bond breaks in the fatigue crack initiation phase when its fatigue cycle number becomes larger than N_1 .

$$N_1 \geq \frac{1}{C_1[1-(1-D_c)^{B+1}]^{A(\tilde{\sigma})}(\dfrac{\sigma_a}{M(\bar{\sigma})(1-D_c)})^B} \tag{23}$$

where the first bond breaks with cyclic bond in fatigue crack initiation, new static solutions for other bonds are calculated in the same cycle.

4.3. Criterion from Fatigue Multi-crack Initiation to Propagation

As shown in Fig. 11(a), the fatigue multi-crack initiation and propagation phase are described in a peridynamic solid. The mechanism of multi-crack initiation and propagation are different. During the fatigue multi-crack initiation, each bond strain is independent of the cycle number. However, a bond strain is changing over time as the bond transit to the fatigue crack propagation phase. As shown in Fig. 11(b), for the given point $x_{(k)}$, within the horizon of point $x_{(j)}$, the bond ξ_{12} (denoted as sky-blue) transit to the fatigue crack growth phase as the point damage $D_j(x_j)$ satisfies the following expression.

$$D_j(x_j) \geq 0.5 \tag{24}$$

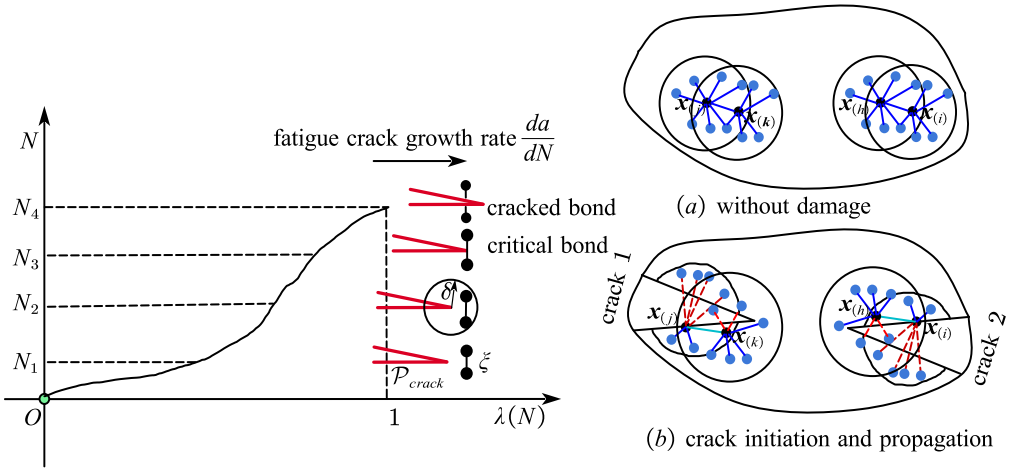

Figure 11. The crack tip analysis of bond damage

Preprints (www.preprints.org) | NOT PEER-REVIEWED | Posted: 10 May 2022 doi:10.20944/preprints202205.0140.v1

5. Validation Procedure of Numerical Solution Method

5.1. Quasi-Static Solution for each Cyclic Loading

Although the equation of motion of the peridynamic theory is in dynamic form, it can still be applicable to solve quasi-static or static problems by using a dynamic relaxation technique. The peridynamic control equation for fatigue cracking is integral-different. As for compression-compression fatigue loading simulation, the maximal loading condition is necessary.

Whenever some bonds break in a loading cycle, the new quasi-static solution is calculated at the same cycle until no bonds break. To solve quasi-static or static problems, the Adaptive Dynamic Relaxation is used for the multiple crack simulation problems. According to the ADR method, the PD equation of motion is written as a set of ordinary differential equations for all material points in the system by introducing new fictitious inertia and damping terms.

$$\boldsymbol{D}\ddot{\boldsymbol{U}}(\boldsymbol{X},t)+\zeta\boldsymbol{D}\dot{\boldsymbol{U}}(\boldsymbol{X},t)=\boldsymbol{F}(\boldsymbol{U},\boldsymbol{U}',\boldsymbol{X},\boldsymbol{X}') \tag{25}$$

where $\boldsymbol{D}$ is the fictitious diagonal density matrix and ζ is the damping coefficient, $\boldsymbol{X}$ and $\boldsymbol{U}$ are initial position and displacement vector for all the material points in the configuration body and they can be expressed as

$$\begin{cases}\boldsymbol{X}^T=\{\boldsymbol{x}_1,\boldsymbol{x}_2,\cdots,\boldsymbol{x}_N\}\\ \boldsymbol{U}^T=\{\boldsymbol{u}(\boldsymbol{x}_1,t),\boldsymbol{u}(\boldsymbol{x}_2,t),\cdots,\boldsymbol{u}(\boldsymbol{x}_N,t)\}\end{cases} \tag{26}$$

where $\boldsymbol{N}$ is the number of all the material points in the configuration body. Finally, the vector $\boldsymbol{F}$ is composed of PD interaction and body forces and its k^{th} component.

$$\boldsymbol{F}_{(k)}=\sum_{j=1}^{M}\left(t_{(k)(j)}-t_{(j)(k)}\right)\left(v_{cj}V_{(j)}\right)+\boldsymbol{b}_{(k)} \tag{27}$$

where M is the total number of material points within the horizon of a material point $\boldsymbol{x}_{(k)}$, v_{cj} is the volume correction factor for the material point $\boldsymbol{x}_{(j)}$. The velocities and displacements for the next time step are expressed as follows.

$$\begin{cases}\boldsymbol{V}^{n+1/2}=\dfrac{\left(\left(2-\zeta^n\Delta t\right)\mathbf{V}^{n-1/2}+2\Delta t\boldsymbol{D}^{-1}\boldsymbol{F}^n\right)}{2+\zeta^n\Delta t}\\ \boldsymbol{U}^{n+1}=\boldsymbol{U}^n+\boldsymbol{V}^{n+1/2}\Delta t\end{cases} \tag{28}$$

where n is the n^{th} iteration. The diagonal elements of the density matrix, $\boldsymbol{D}$, can be expressed as

$$\gamma_{kk}\geqslant\frac{1}{4}\Delta t^2\sum_j\left|\mathcal{J}_{kj}\right| \tag{29}$$

where $\mathcal{J}_{kj}$ is the stiffness matrix of the current structure for the small displacement assumption.

$$\sum_j\left|\mathcal{J}_{kj}\right|=\sum_{j=1}^{M}\frac{\left|\xi_{(k)(j)}\cdot\mathbf{e}\right|}{\left|\xi_{(k)(j)}\right|}\frac{4\delta}{\left|\xi_{(k)(j)}\right|}\left\{\frac{1}{2}\frac{ad^2\delta}{\left|\xi_{(k)(j)}\right|}\left(v_{ck}V_k+v_{cj}V_j\right)+b\right\} \tag{30}$$

where **e** is a unit vector.

5.2. Equivalent Fatigue Parameters Between PD and EPFM

Each step of crack growth requires a driving force, which guides the fatigue crack path. Naturally, this driving force named stress intensity factor. Because of the complexity in mathematics and physics, solving the three-dimensional dynamic stress intensity factors is certainly limited in mechanics. In the non-ordinary state-based peridynamic theory, there is no concept of this driving force. To better characterize the propagating crack-tip fields, an equivalent stress intensity factor $\hat{\lambda}_{equ}$ can be expressed as follows

$$\hat{\lambda}_{equ}=\int_\Gamma\left(Wdy-T_i\frac{\partial u_i}{\partial x}ds\right)=\frac{2E}{\left(1-\nu^2\right)}\sum_{i=I,II,II}\int_i\left(W_idy-w_ids\right) \tag{31}$$

Preprints (www.preprints.org) | NOT PEER-REVIEWED | Posted: 10 May 2022 doi:10.20944/preprints202205.0140.v1

where $x=x_1$, $y=x_2$, and $z=x_3$ are 3D Cartesian coordinates with origin at the fatigue crack tip, $\hat{\lambda}_{equ}$ is a contour integral evaluated counterclockwise along a crack surface, $T_i=\sigma_{ij}n_j$ is the traction vector along the crack surface, with the outward unit normal vector σ_{ij} and n_j, u_i is a displacement vector and ds is an element of the crack surface. By taking the surface integration, the relationship between the displacement and fatigue crack is built. Each step of crack growth can be obtained from the relationship.

5.3. The Whole Process to Simulate Fatigue Multi-crack Initiation and Propagation

Based on the comparison and analysis of the classical fatigue crack simulation algorithm and the peridynamic one, the simulation process for the multi-crack initiation and propagation is built, as shown in Fig. 12.

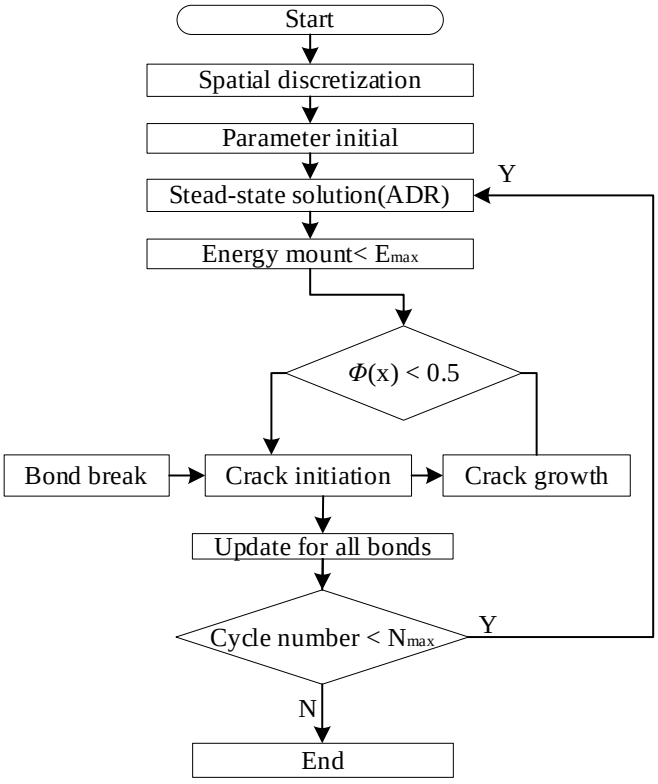

Figure 12. Flowchart of the multiple cracks simulation

6. Fatigue Experiment

6.1. Structural Fatigue Testing Platform with Overalls Tools

As shown in Fig. 13, the fatigue experiment was carried out in a structural test platform with overalls tools, which the floor model servo-hydraulic dynamic test system provides axial and torsion load on the aircraft wing corner box. The servo-hydraulic dynamic test platform has an axial load capacity of ±100KN (±22.4kip) and a torque capacity of ±1000Nm (±8850in-lb), with an axial actuator stroke of 50 mm and a rotary stroke of 45°. Since, these tests are being conducted in tension only, the stress ratio, R, is chosen to be close to but not exactly zero such that R=0.1. Thus, $\sigma_{min}=R*\sigma_{max}$, where σ_{max} is the desired maximum stress. Load ratio R is defined as the ratio of the minimum and maximum loads during the compression-compression fatigue loading. Without environmental effects, the load ratio has a more significant effect on the stages I and III fatigue crack growth rates than in stage II. The fatigue test characteristics are 6Hz frequency and 0.1 as the ratio of minimum to maximum loading in tensile regime.

Preprints (www.preprints.org) | NOT PEER-REVIEWED | Posted: 10 May 2022 doi:10.20944/preprints202205.0140.v1

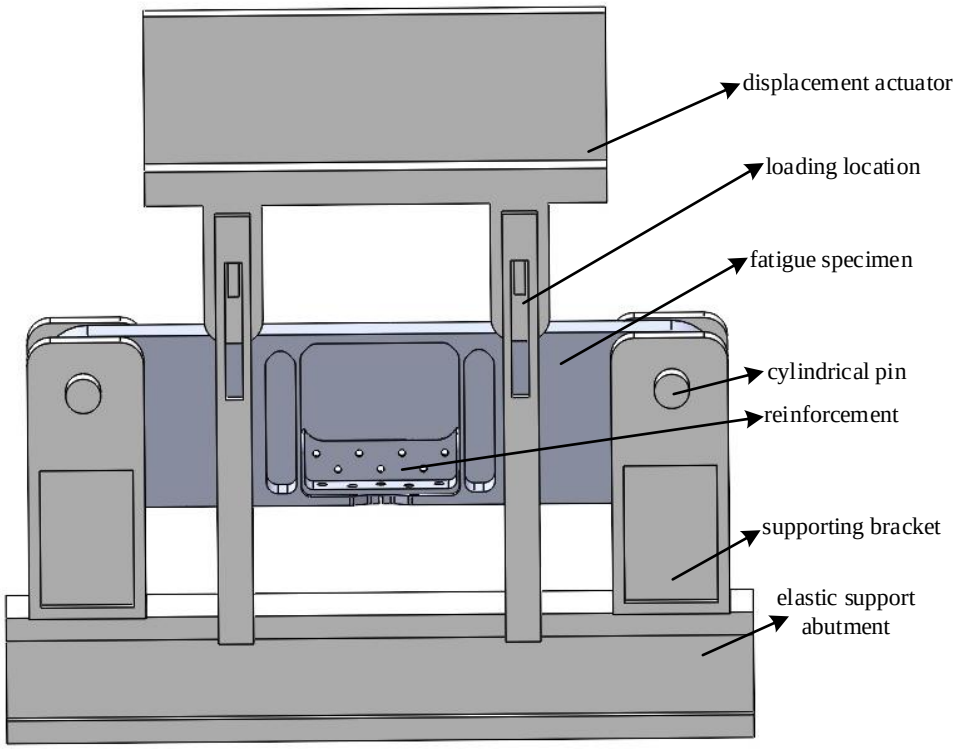

Figure 13. Fatigue test platform for the tension only experiment

As shown in Fig. 14, the dynamic fatigue testing system, which comes with fatigue test procedure to provide full system control from a personal computer (PC), including waveforms generated by function generators in both axes, signal calibration strategy and related impact factors, limit set up by human rationality and system range, and status monitoring by master system display interface module.

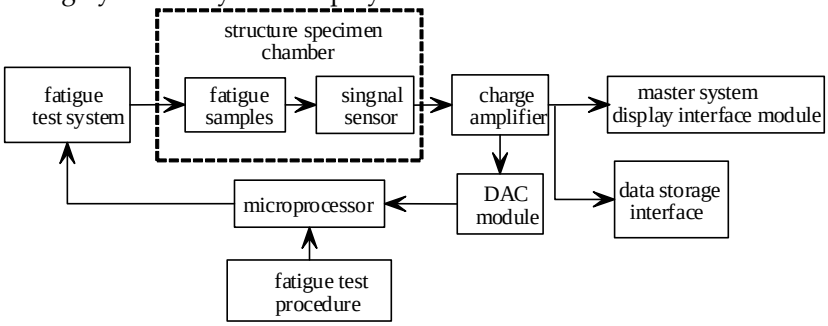

Figure 14. Configuration of the structure fatigue test platform

6.2. Sample Dimension Description and Input Parameters

As shown in Fig. 15, computer data recording system and crack length measurement is used for the multi-crack initiation and propagation. The aircraft wing corner box and the reinforcement are bolted together. A u-shaped notch is in the middle of the aircraft wing corner box, which also means that the notch is the weak part of the sample without considering other factors under compression-compression fatigue loading. The maximum percentages of the various specified elements are shown in Tab. 1. The basic mechanical properties for the aluminium alloy material are shown in Tab. 2. The loading parameters are shown in Tab. 3.

Preprints (www.preprints.org) | NOT PEER-REVIEWED | Posted: 10 May 2022 doi:10.20944/preprints202205.0140.v1

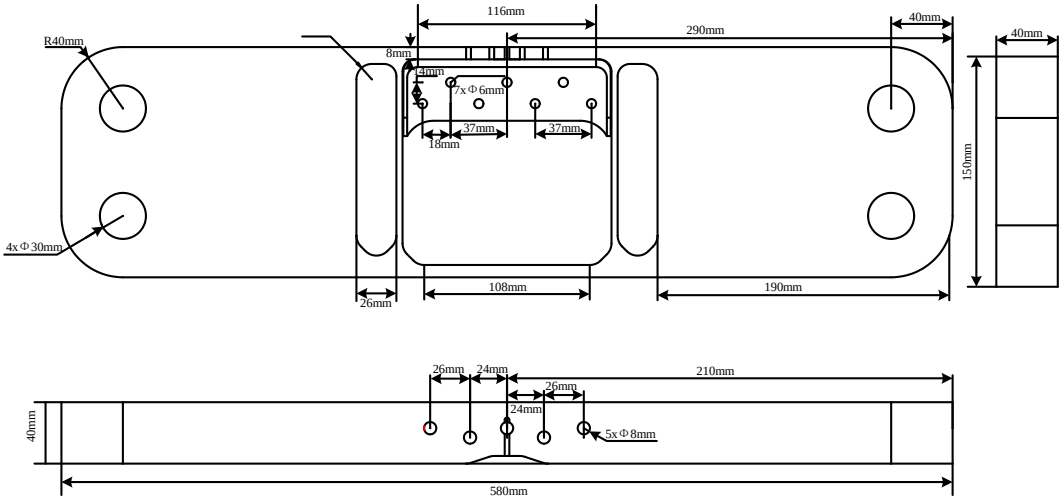

Figure 15. Fatigue structure sample

Table 1. The maximum percentages of the various specified elements

Zn%	Cu%	Mg%	Mn%	Fe%	Si%	Cr%	Ti%	Al%
5.75	1.57	2.49	0.29	0.28	0.27	0.18	< 0.1	Others

Table 2. Basic mechanical properties of the aircraft wing corner box material at room temperature

Name	E/GPa	$\sigma_{0.2}$/MPa	σ_b/MPa	δ%	Fatigue Strength/MPa	Density g/cm^3	Poisson' Ratio	Brinell Hardness /HB	Shear Modulus/GPa	Shear Strength/MPa
7075-T6	70	480	560	7.9	160	3.0	0.32	150	26	330

Table 3. Loading parameters

σ_a/MPa	τ_a/MPa	σ_{equ}/MPa	R_a	F_{max}/KN	f/HZ
340	196.3	480.83	$\sqrt{3}$	9.6	6

6.3. Crack Morphology and Data Recording

The multi-crack morphology of the fatigue sample is shown in Fig. 16.

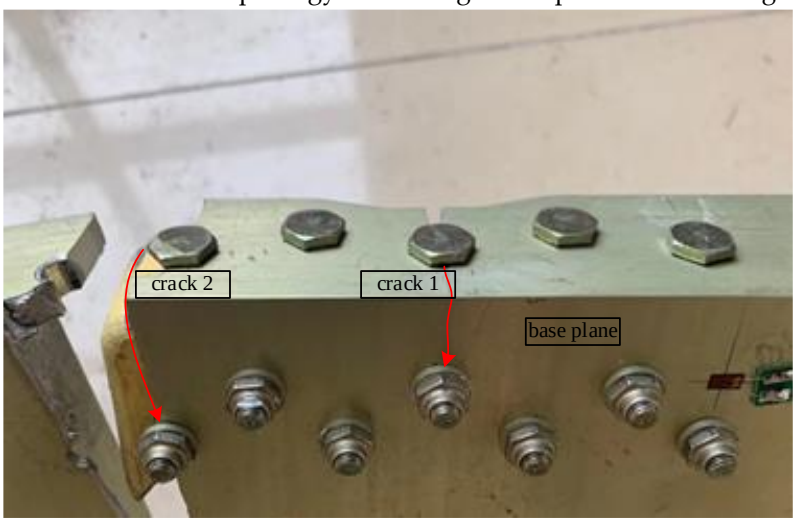

Figure 16. Macro multi-crack characteristics of the fatigue sample

Preprints (www.preprints.org) | NOT PEER-REVIEWED | Posted: 10 May 2022 doi:10.20944/preprints202205.0140.v1

The number of cycles for the crack 1 and crack 2 are shown Tab. 4

Samples	Crack 1		Crack 2	
NO	initiation	propagation	initiation	propagation
7075-T6-1	24146	23854	28036	18558
7075-T6-2	22334	24706	27586	15414
7075-T6-3	30036	18234	29766	12048
7075-T6-4	29058	19028	35696	10068
7075-T6-5	20048	25703	34330	10268
7075-T6-6	24100	30854	25004	18500

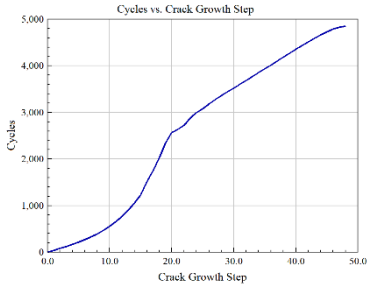

(a) The cycle number of the crack 1

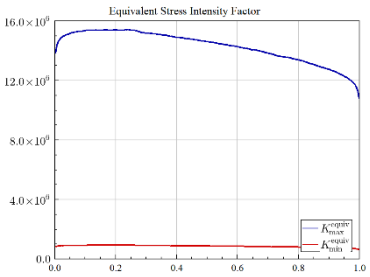

(b) Equivalent SIF in step 5

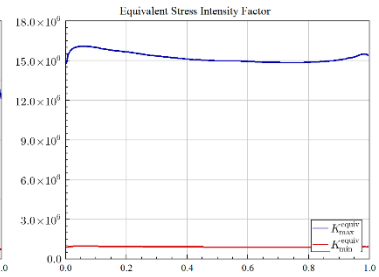

(c) Equivalent SIF in step 20

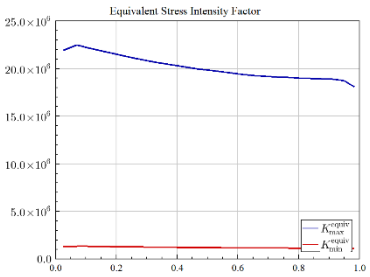

(d) Equivalent SIF in step 30

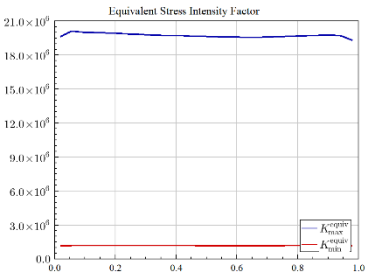

(e) Equivalent SIF in step 35

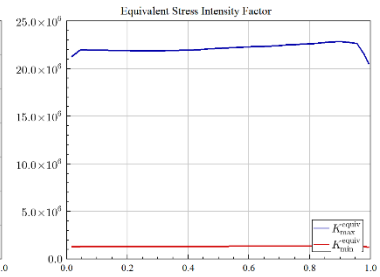

(f) Equivalent SIF in step 45

Figure 17. Equivalent stress intensity factors in each specified iteration for crack 1. (**a**) Cycle number vs. crack growth step; (**b**) λ_{equ} at crack front in nstep=5; (**c**) λ_{equ} at crack front in nstep=20; (**d**) λ_{equ} at crack front in nstep=30; (**e**) λ_{equ} at crack front in nstep=35; (**f**) λ_{equ} at crack front in nstep=45

Preprints (www.preprints.org) | NOT PEER-REVIEWED | Posted: 10 May 2022 doi:10.20944/preprints202205.0140.v1

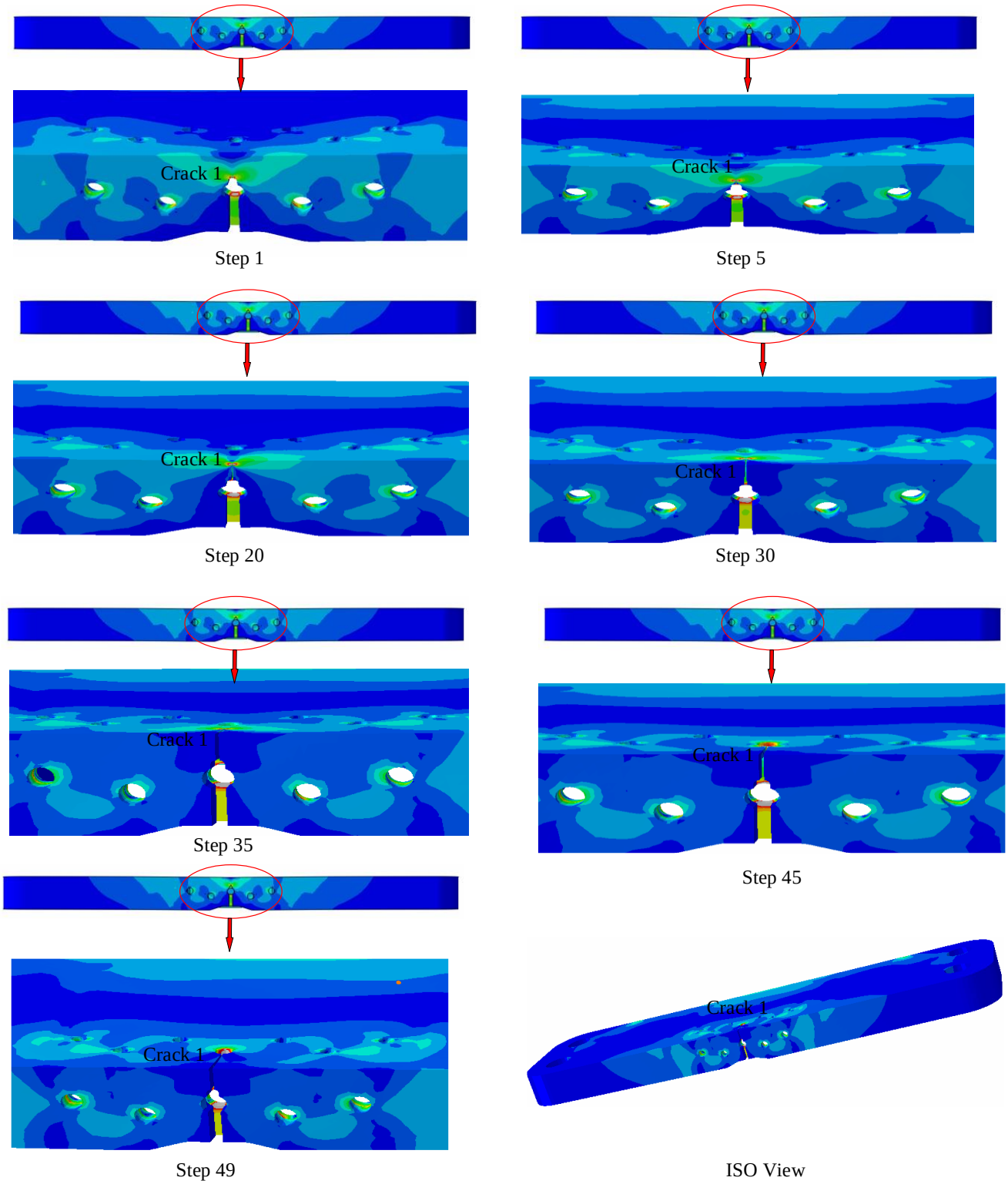

Figure 18. Simulation results of the crack 1 based on the peridynamic fatigue model (**a**) The fatigue crack propagation in nstep=1; (**b**) The fatigue crack propagation in nstep=5; (**c**) The fatigue crack propagation in nstep=20; (**d**) The fatigue crack propagation in nstep=30; (**e**) The fatigue crack propagation in nstep=35; (**f**) The fatigue crack propagation in nstep=45; (**g**) The fatigue crack propagation in nstep=49;

Preprints (www.preprints.org) | NOT PEER-REVIEWED | Posted: 10 May 2022 doi:10.20944/preprints202205.0140.v1

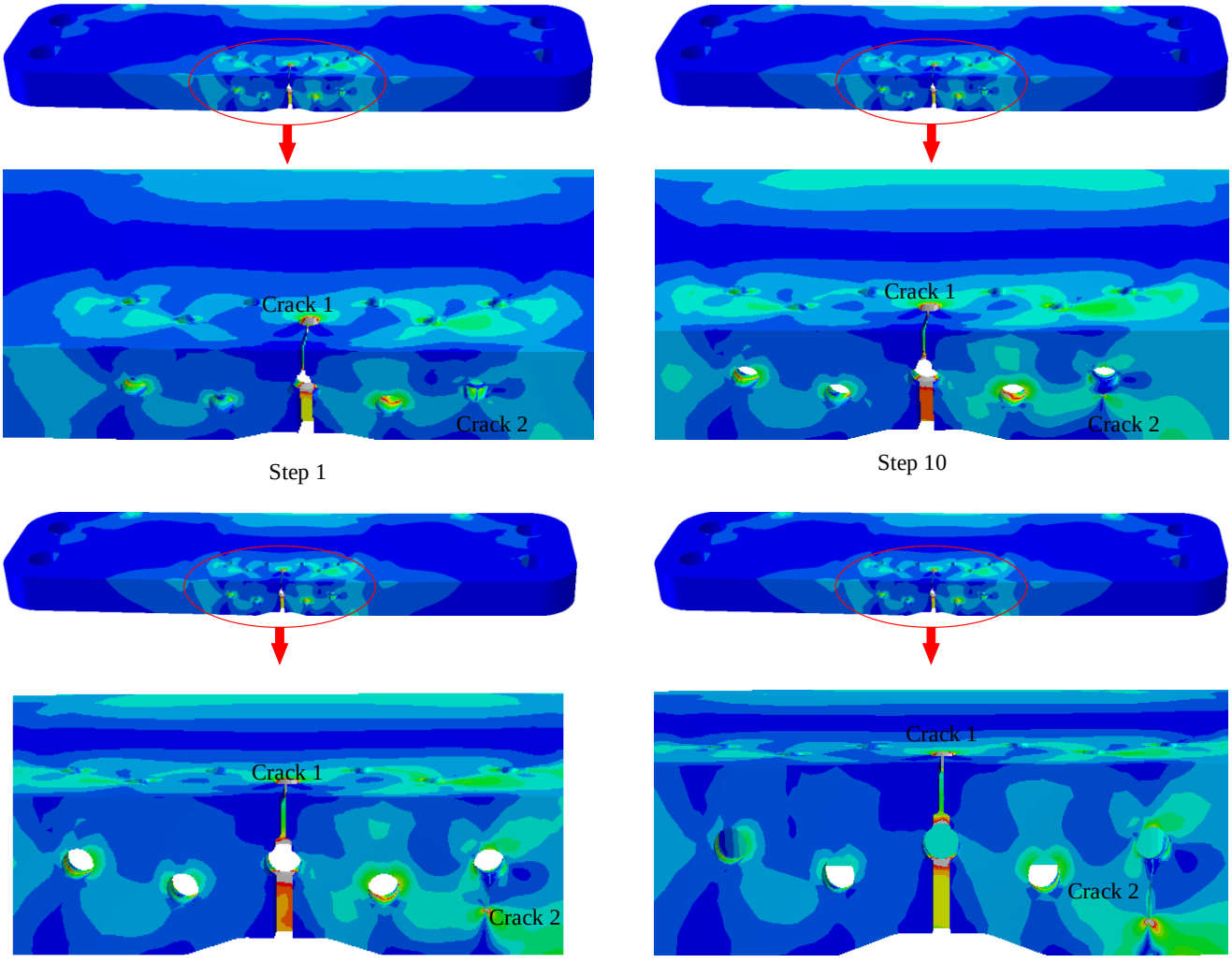

Figure 19. Simulation results of the crack 1 and crack 2 based on the peridynamic fatigue model. (**a**) The fatigue crack propagation in nstep=1; (**b**) The fatigue crack propagation in nstep=10; (**c**) The fatigue crack propagation in nstep=15; (**d**) The fatigue crack propagation in nstep=19;

Preprints (www.preprints.org) | NOT PEER-REVIEWED | Posted: 10 May 2022 doi:10.20944/preprints202205.0140.v1

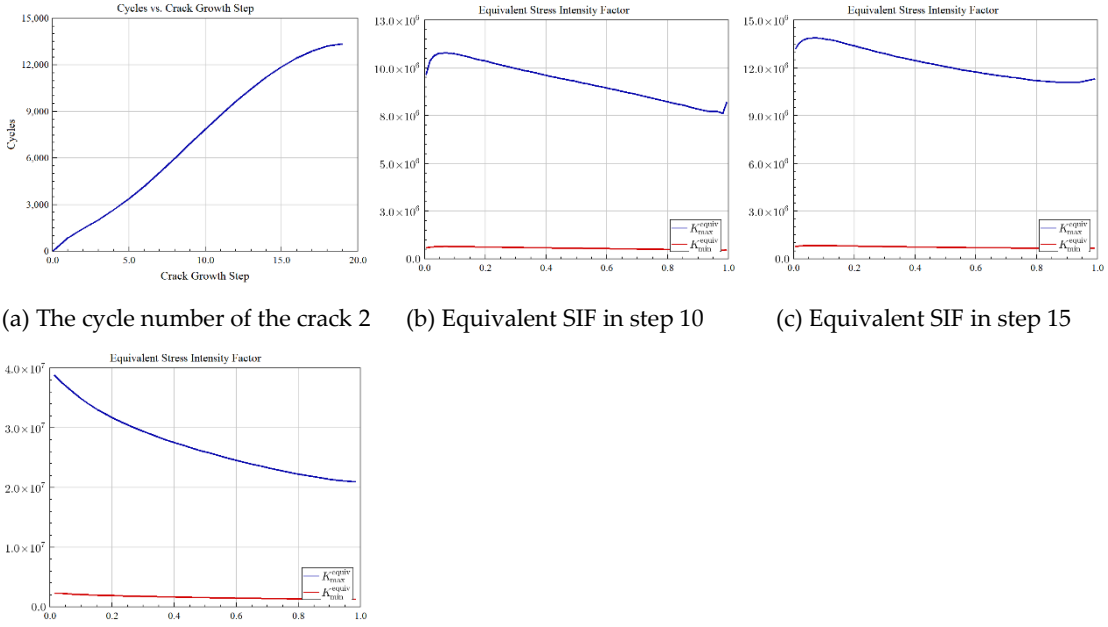

(a) The cycle number of the crack 2 (b) Equivalent SIF in step 10 (c) Equivalent SIF in step 15

(d) Equivalent SIF in step 18

Figure 20. Equivalent stress intensity factors in each specified iteration for crack 2. (**a**) Cycle number vs. crack growth step; (**b**) λ_{equ} at crack front in nstep=10; (**c**) λ_{equ} at crack front in nstep=15; (**d**) λ_{equ} at crack front in nstep=18

6.4. Data Analysis and Countermeasures

As shown in Fig. 16, using macro monitoring technology, it can be seen that the aircraft wing corner box have a multiple crack, crack 1 and crack 2. The cycle number of the crack 1 and crack 2 are shown in Tab. 4.

As shown in Tab. 4, the average fatigue cycle is 30069 for the crack 1, and the average fatigue cycle is 22106 for the crack 2.

As shown in Fig. 18, the crack 1 path vs. Fig. 16, the angle between crack 1 and the base plane is about 89.5°; As shown in Fig. 19, the crack 2 path vs. Fig. 16, the angle between crack 2 and the base plane is about 87.6°. This simulation result has a good correlation with the average test result, as shown in Fig. 16.

As shown in Fig. 17 and Fig. 18, the value of the equivalent stress intensity factor λ_{equ} becomes larger as the number of iterations increases.

7. Conclusions

(1) To evaluate and predict the fatigue life of the aircraft wing corner box under compression-compression fatigue loading, a non-ordinary state based peridynamics fatigue model was proposed. The multiple fatigue cracks initiate and propagate naturally without extra criteria with this constitutive model for fatigue.

(2) The proposed non-ordinary state based peridynamics fatigue model has no notion of scale, or it releases the scale constraints. The evolution of fatigue crack shows micro and macro scale including multiple crack initiation, propagation, and fracture.

(3) The two of the crack, crack 1 and crack 2, converge and grow into the main crack respectively, which expands to the macroscopic visible morphology.

(4) The natural propagation of the crack can be realized without the need for additional crack propagation criteria, and the distribution and quantitative analysis of the fatigue life can be obtained.

Author Contributions: Conceptualization, J.H. and G.W.; methodology, G.W. and R.C.; software, X.Z. and R.C.; validation, J.H., G.W. and X.Z.; formal analysis, J.H. and G.W.; investigation, J.H. and X.Z.; resources, J.H. and R.C.; data curation, X.Z. and G.W.; writing—original draft preparation, J.H. and R.C.; writing—review and editing, J.H and R.C.; visualization, J.H. and R.C.; supervision, W.C.; project administration, W.C.; funding acquisition, W.C. All authors have read and agreed to the published version of the manuscript.

Funding: This research was funded by TEN THOUSAND TALENTS PROGRAM, grant number 2018R008.

Institutional Review Board Statement: Not applicable

Informed Consent Statement: Not applicable

Data Availability Statement: The data sets generated and/or analyzed during the current study are available from the corresponding author on reasonable request.

Conflicts of Interest: The authors declare no conflict of interest.

References

1. Pineau A, Benzerga A A, Pardoen T. Failure of metals III : Fracture and fatigue of nanostructured metallic materials [J]. Acta Materialia, 2016, 107.
2. Forrest P G. Fatigue of metals [M]. Elsevier, 2013.
3. Stephens R I, Fatemi A, Stephens R R, et al. Metal fatigue in engineering [M]. John Wiley & Sons, 2000.
4. Man J, Obrtlik K, Blochwitz C, et al. Atomic force microscopy of surface relief in individual grains of fatigued 316L austenitic stainless steel [J]. Acta Materialia, 2002, 50(15): 3767-3780.
5. Alfyorova E, Lychagin D. Self-organization of plastic deformation and deformation relief in FCC single crystals [J]. Mechanics of Materials, 2018, 117: 202-213.
6. Heczko M, Polák J, Kruml T. Microstructure and dislocation arrangements in Sanicro 25 steel fatigued at ambient and elevated temperatures [J]. Materials Science and Engineering: A, 2017, 680: 168-181.
7. Makin M. Electron displacement damage in copper and aluminium in a high voltage electron microscope [J]. Philosophical Magazine, 1968, 18(153): 637-653.
8. Kelly A, Knowles K M. Crystallography and crystal defects [M]. John Wiley & Sons, 2020.
9. Nagase T, Umakoshi Y. Electron irradiation induced crystallization of the amorphous phase in Zr-Cu based metallic glasses with various thermal stability [J]. Materials Transactions, 2004, 45(1): 13-23.
10. Oskay C, Fish J. Fatigue life prediction using 2-scale temporal asymptotic homogenization [J]. International Journal for Numerical Methods in Engineering, 2004, 61(3): 329-359.
11. Fish J: Multiscale modeling and simulation of composite materials and structures, Multiscale methods in computational mechanics: Springer, 2011: 215-231.
12. Ortolano González J M, Hernández Ortega J A, Oliver Olivella X. A comparative study on homogenization strategies for multiscale analysis of materials [M]. Centre Internacional de Mètodes Numèrics en Enginyeria (CIMNE), 2013.
13. Yuan Z, Fish J. Toward realization of computational homogenization in practice [J]. International Journal for Numerical Methods in Engineering, 2008, 73(3): 361-380.
14. Guidault P-A, Allix O, Champaney L, et al. A two-scale approach with homogenization for the computation of cracked structures [J]. Computers & structures, 2007, 85(17-18): 1360-1371.
15. Schijve J. Fatigue damage in aircraft structures, not wanted, but tolerated? [J]. International Journal of Fatigue, 2009, 31(6): 998-1011.
16. Murakami Y, Miller K. What is fatigue damage? A view point from the observation of low cycle fatigue process [J]. International Journal of Fatigue, 2005, 27(8): 991-1005.
17. Schijve J. Fatigue of structures and materials [M]. Springer, 2009.
18. Jung J, Seok J. Fatigue crack growth analysis in layered heterogeneous material systems using peridynamic approach [J]. Composite Structures, 2016, 152: 403-407.
19. Jung J, Seok J. Mixed-mode fatigue crack growth analysis using peridynamic approach [J]. International Journal of Fatigue, 2017, 103: 591-603.
20. Ondráček J, Materna A. FEM evaluation of the dissipated energy in front of a crack tip under 2D mixed mode loading condition [J]. Procedia materials science, 2014, 3: 673-678.
21. Horníková J, Šandera P, Žák S, et al. Specimens for simultaneous mode II, III and II+ III fatigue crack propagation: Elasto-plastic solution of crack tip stress-strain field [C]. Advanced Materials Research, 2014: 1585-1590.
22. Shlyannikov V, Tumanov A, Boychenko N. Surface crack growth rate under tension and bending in aluminum alloys and steel [J]. Procedia Engineering, 2016, 160: 5-12.

23. Solanki K, Daniewicz S, Newman Jr J. Finite element analysis of plasticity-induced fatigue crack closure: an overview [J]. Engineering Fracture Mechanics, 2004, 71(2): 149-171.
24. Antunes F, Rodrigues D. Numerical simulation of plasticity induced crack closure: Identification and discussion of parameters [J]. Engineering Fracture Mechanics, 2008, 75(10): 3101-3120.
25. Jiang Y, Feng M, Ding F. A reexamination of plasticity-induced crack closure in fatigue crack propagation [J]. International Journal of Plasticity, 2005, 21(9): 1720-1740.
26. Dunne F. Fatigue crack nucleation: Mechanistic modelling across the length scales [J]. Current Opinion in Solid State and Materials Science, 2014, 18(4): 170-179.
27. Espinosa H D, Zavattieri P D. A grain level model for the study of failure initiation and evolution in polycrystalline brittle materials. Part I: Theory and numerical implementation [J]. Mechanics of Materials, 2003, 35(3-6): 333-364.
28. Raghami E, Schrank C, Kruhl J H. 3D modelling of the effect of thermal-elastic stress on grain-boundary opening in quartz grain aggregates [J]. Tectonophysics, 2020, 774: 228242.
29. Simkin B, Crimp M, Bieler T. A factor to predict microcrack nucleation at γ–γ grain boundaries in TiAl [J]. Scripta Materialia, 2003, 49(2): 149-154.
30. Wei B, Liu Z, Nong B, et al. Microstructure, cracking behavior and mechanical properties of René 104 superalloy fabricated by selective laser melting [J]. Journal of Alloys and Compounds, 2021, 867: 158377.
31. Dunne F, Wilkinson A, Allen R. Experimental and computational studies of low cycle fatigue crack nucleation in a polycrystal [J]. International Journal of Plasticity, 2007, 23(2): 273-295.
32. Mcdowell D, Dunne F. Microstructure-sensitive computational modeling of fatigue crack formation [J]. International journal of fatigue, 2010, 32(9): 1521-1542.
33. Mcdowell D L. Simulation-based strategies for microstructure-sensitive fatigue modeling [J]. Materials Science and Engineering: A, 2007, 468: 4-14.
34. Shenoy M, Tjiptowidjojo Y, Mcdowell D. Microstructure-sensitive modeling of polycrystalline IN 100 [J]. International Journal of Plasticity, 2008, 24(10): 1694-1730.
35. Tinga T, Brekelmans W, Geers M. Time-incremental creep–fatigue damage rule for single crystal Ni-base superalloys [J]. Materials Science and Engineering: A, 2009, 508(1-2): 200-208.
36. Tschopp M, Tucker G, Mcdowell D. Atomistic simulations of tension–compression asymmetry in dislocation nucleation for copper grain boundaries [J]. Computational Materials Science, 2008, 44(2): 351-362.
37. Madenci E, Oterkus E: Peridynamic theory, Peridynamic theory and its applications: Springer, 2014: 19-43.
38. Das S, Hoffarth C, Ren B, et al. Simulating the fracture of notched mortar beams through extended finite-element method and peridynamics [J]. Journal of Engineering Mechanics, 2019, 145(7): 04019049.
39. Silling S A, Lehoucq R B. Peridynamic theory of solid mechanics [J]. Advances in applied mechanics, 2010, 44: 73-168.
40. Silling S A, Epton M, Weckner O, et al. Peridynamic states and constitutive modeling [J]. Journal of elasticity, 2007, 88(2): 151-184.
41. Silling S A, Askari E. A meshfree method based on the peridynamic model of solid mechanics [J]. Computers & structures, 2005, 83(17-18): 1526-1535.
42. Chen L Y, Richter G, Sullivan J P, et al. Lattice anharmonicity in defect-free Pd nanowhiskers [J]. Physical Review Letters, 2012, 109(12): 125503.
43. Wei X, Naraghi M, Espinosa H D. Optimal length scales emerging from shear load transfer in natural materials: application to carbon-based nanocomposite design [J]. ACS nano, 2012, 6(3): 2333-2344.
44. Rahman R, Foster J T, Haque A. A multiscale modeling scheme based on peridynamic theory [J]. International Journal for Multiscale Computational Engineering, 2014, 12(3).
45. Oterkus E, Guven I, Madenci E. Fatigue failure model with peridynamic theory [C]. 2010 12th IEEE Intersociety Conference on Thermal and Thermomechanical Phenomena in Electronic Systems, 2010: 1-6.
46. Silling S A, Askari A. Peridynamic model for fatigue cracking [J]. SAND2014-18590. Albuquerque: Sandia National Laboratories, 2014.
47. Zhang G, Le Q, Loghin A, et al. Validation of a peridynamic model for fatigue cracking [J]. Engineering Fracture Mechanics, 2016, 162: 76-94.
48. Hu Y, Madenci E. Peridynamics for fatigue life and residual strength prediction of composite laminates [J]. Composite Structures, 2017, 160: 169-184.
49. Baber F, Guven I. Solder joint fatigue life prediction using peridynamic approach [J]. Microelectronics Reliability, 2017, 79: 20-31.
50. Basoglu M F, Zerin Z, Kefal A, et al. A computational model of peridynamic theory for deflecting behavior of crack propagation with micro-cracks [J]. Computational Materials Science, 2019, 162: 33-46.
51. Zhu N, De Meo D, Oterkus E. Modelling of granular fracture in polycrystalline materials using ordinary state-based peridynamics [J]. Materials, 2016, 9(12): 977.
52. Silling S A. Reformulation of elasticity theory for discontinuities and long-range forces [J]. Journal of the Mechanics and Physics of Solids, 2000, 48(1): 175-209.

 doi:10.20944/preprints202205.0140.v1

53. Han J, Chen W. An ordinary state-based peridynamic model for fatigue cracking of ferrite and pearlite wheel material [J]. Applied Sciences, 2020, 10(12): 4325.